Article

Using Modified Chestnut-Nano Shell for Removal of Diclofenac from Aqueous Solution

Rounak M. Shariff*

*Department of Chemistry College of Science, Salahaddin University of -Erbil, Kurdistan Region, Iraq

rounak.shariff@su.edu.krd

Abstract

In this study, the adsorption of an anti-inflammatory drug diclofenac (Dc) by modified chestnut peels. Chestnut peels (CP), acid chestnut peels carbonized (ACSPC), and chestnut peels carbonized impregnation by ferric and nickel (II) oxide ($NiFe_2O_4$-CPC) nanocomposite, investigated to remove Dc from an aqueous solution. Batch experiments were conducted for adsorption capacity for Dc from an aqueous solution using the modified chestnut peels. The modified chestnut peels and morphological changes after adsorption were characterization by the following techniques: FTIR, XRD, SEM, and EDX respectively. The kinetic model; pseudo-second-order and isothermal model; Langmuir demonstrated the adsorption processes on adsorbents. The K_2, q_e, and R^2 values were in the range (0.303 to 1.20) $g\mu g^{-1}min^{-1}$, (0.039 to 0.160) mgg^{-1}, and (0.712-0.972) respectively, at three different temperatures 298, 308, and 318 K. While for Langmuir isotherm the value of K_L, C_m, and R^2 in the range (0.014–0.024) L mg^{-1}, (14.286-16.667) mg g^{-1}, and (0.737-0.982) respectively for Dc on the adsorbents. The thermodynamic parameters revealed that the spontaneous and exothermic Dc adsorption process on the modified chestnut peels and the nanocomposite, also having good adsorption efficiency for removing pharmaceutical pollution from aqueous solutions could be used for water treatments.

Keywords: adsorption, diclofenac, $NiFe_2O_4$-Nano, thermodynamic.

1. Introduction

Many pollutants are antibiotics, persistent organic pollutants, and other industrial chemicals. They are very complex organic matter, although they exist in water with low content but with great harm to the environment. The pharmaceutical drug, such as antibiotics and anti-inflammatories, which have potential threats to human health and the aquatic environment [1]. The existence of these pollutants which are transforming into environmental media through the food chain after being accumulated by organisms have potential impacts on the human health and environment [2].

The diclofenac (Dc) anti-inflammatory and painkillers drugs such as this drug have been frequently seen in surface water and wastewater [3]. It's consumed largely by the human population and expelled in urine, basically, which affects the ecological environment [4]. Several physicochemical methods are used to remove Dc from water solution: electrochemical process [5]. Adsorption process and oxidation methods [6]. The most advantageous of the adsorption processes is using agricultural waste, high adsorption efficiency, a wide processing range, widely surfaced phenomenon information, and finally a method for equilibrium separation [7]. The low cost, simple processes, ease of release, and hazardous chemicals not allowing forming were the advantages of the adsorption process for pollutant removal from the wastewater [8]. The activated carbon widely used adsorbent has many advantages: high surface area, high porous structure, and removal of

pollutants from wastewater, like organic (pesticides and dyes), and inorganic (heavy metals) materials [9]. Different types of biomass wastes have been used as adsorbents to remove Dc: Pine tree [10], Tea waste [11], Potato peel waste [12], Coconut shell [13], Orange peels [14], and activated carbon [15, 16]. The adsorption mechanism of organic compounds on activated carbon: electrostatic attraction, hydrophobic interaction, and electron donor-acceptor interactions [17, 18].

The adsorption process using nanomaterials exhibits high surface activity, high surface area, and demonstrates high effective interactions with various chemicals [19, 20]. The applications of various spinel magnetic nanoparticles such as $NiFe_2O_4$ have been investigated as magnetic adsorbents [21, 22]. The advantage of nickel ferrite is due to its catalytic behavior, high permeability, high chemical and electrochemical stability, high saturation magnetization, low conductivity high Curie temperature, that consider nickel ferrite an efficient adsorbent [23].

The world wide, human life and other living beings depended on water, which is the most effective substance. Using water for various industries that are contaminated with various chemicals. The present work modified Chestnut peels; (CP), (ACSPC), and ($NiFe_2O_4$-CPC) nanocomposites were obtained, and investigated their capacity of adsorption on Dc from aqueous solution. This goal is determined by the removal of pollution from various industrial effluents. The adsorbents were characterized regarding their pore structure and surface properties by FTIR, XRD, SEM, and EDX. The batch adsorption experiments: pH, adsorbent dosage, contact time, and initial Dc concentration were optimized employing response surface methodology indicting the potential of modified chestnut peels for Dc removal from aqueous solutions has been used. The mechanism and nature of Dc adsorption with modified Chestnut peels using adsorption kinetics, isotherm, and thermodynamic studies were conducted to describe the removal. Furthermore, Dc adsorption-desorption cycles an adsorbent reuse and recycle test were conducted for five consecutive.

2. Experimental

2.1. Materials

Diclofenac sodium 98% (Dc), Boric acid (H_3BO_3), Sodium hydrochloride (NaCl), and methanol (99% purity), Sulfuric acid (98%, Sp.gr. 1.84) and Nickel(II) chloride hex hydrate [$NiCl_2.6H_2O$]. Ferric chloride hexahydrate [$FeCl_3.6H_2O$]. Sodium hydroxide pellets [NaOH] were purchased from BDH. The chemicals and other analytical materials used were grade-used without further purification in this study, and all solutions and standards were prepared using de-ionized water.

2.2.Instrumentation

Tabletop pH Meter with Multi parameters from China (PHS-550). Spectrophotometer (UV-Visible/Visible Spectrophotometer AE-S60), with a 1.0 cm path length quartz cell, used for absorption measurements. A PerkinElmer LS-45 fluorescence spectrometer (Buckinghamshire, UK) was used for fluorescence measurements. PW, 1730-Philips instrument was used to create the XRD pattern. The Perkin–Elmer

spectrometer was used to record FTIR spectra at room temperature. SEM, EDX image was obtained by TESCAN MIRA III (Czech).

2.3 Adsorbat

Diclofenac sodium (Dc) its chemical name is 2-[(2, 6-dichlorophenyl) amino] benzene acetic acid, mono potassium salt Solubility: Freely soluble in methanol; soluble in ethanol (95%); sparingly soluble in water and in glacial acetic acid; practically insoluble in ether, in chloroform and in toluene. Indications: Orally for symptomatic treatment of osteoarthritis and its Empirical formula is $C_{14}H_{11}Cl_2NO_2$, Na, has molecular weight 296.148 g mol^{-1}, while log K_{ow} = 4.51, and pK_a=4.15. Diclofenac Sodium is a nonosteroidal anti-inflammatory drug used for symptomatic treatment of osteoarthritis, ankylosing spondylitis, primary dysmenorrhea, acute gouty arthritis and for relief of pain, including postoperative (e.g., orthopedic, gynecologic, oral) pain, in adults, the structures were demonstrated in Figure1.

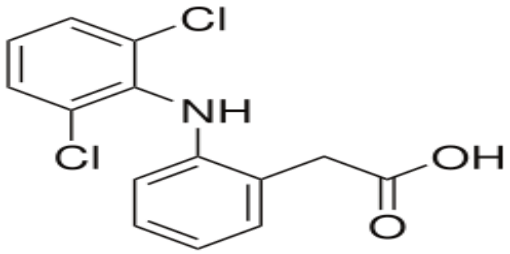

Figure 1. The chemical structure of Diclofenac

The aqueous stock solution of Dc of 1000 mgl^{-1} was prepared, the stock solutions were kept in dark and refrigerated, and then the working solution was prepared. Calibration curves for the antibiotic Dc in aqueous solution were detected at 276 nm [24].

2.4. Adsorbents

The Chestnut peels (CP) were collected, washed with distilled water, air-dried, crushed, and sieved to obtain the desired particle size of 150 µm diameter. Then dried at 110 ^{o}C placed in airtight plastic bags to prevent re-absorption of moisture [24].

The acid chestnut peels carbonized (ACSPC), 50 grams of the selected fraction of Chestnut peels (CP), are impregnated with 0.2M HCl for 24 h by the ratio (1:3) and then washed with deionized water until the pH of the activated carbon reached close to neutral and dried at 110˚C. Then, it was activated at 500˚C for 90 min [24].

Chestnut peels carbonized impregnation by Nickel ferrite nanoparticles ($NiFe_2O_4$-CPC) nanocomposite was synthesized by chemical precipitation method, 16 g of $NiCl_2.6H_2O$, and 28 g of $FeCl_3$.$6H_2O$ were dissolved in 50 mL of deionized water, and then, with continuous stirring for 30 min with heating at 90^{o}C, 30 g of chestnut peels powder was dissolved in 150 mL of deionized water to the solution with continuous stirring for 30 min with heating at 90^{o}C. After that 0.2M sodium hydroxide solution was added drop-wise to the mixture, then continuous stirring at 90°C for 30min. The obtained ($NiFe_2O_4$-CPC) precipitate was then filtered and washed several times with deionised

water. Ethanol solution was used to remove all other ions, and then dried at 110°C in an air oven for 24 hours. Finally, calcinated at 500°C for 90 min and the pure ($NiFe_2O_4$-CPC) nanocomposite preformed [25].

2.5. Batch Adsorption Experiments procedures

The Dc adsorption employed on the surface of the adsorbents each of modified Chestnut peels (CP), (ACSPC), and ($NiFe_2O_4$-CPC) nanocomposites has been concerning. The optimum standard batch equilibrium method obtained at 298K to study: the effects of the initial Dc concentration (25-100) mg L^{-1}, contact time (15-160) min, pH solution (1-10), and adsorbent dosage (0.001- 0.1). Each adsorbent was equilibrated with different Dc concentrations for a duplicate. Another two sets of this solid-solution mixture were prepared, one without Dc used as a blank, and the other without adsorbent used as a control, and placed in the shaker at a speed of 170 rpm. The solid-solution mixtures were centrifuged for 10 min, at 2500 rpm. The absorbance of Dc was calculated based on the adsorption at 276 nm by an UV−vis spectrophotometer. Thermodynamic study done by the same procedure was repeated at 308 K and 318 K. Moreover, we repeated all the experiments three times. The following equations were used to calculate from the results [25].

$$q_e = (C_o - C_e)\frac{V}{W} \quad (1)$$

$$q_t = (C_o - C_t)\frac{V}{W} \quad (2)$$

$$\text{Re}moval\% = \frac{C_o - C_e}{C_o} x100 \quad (3)$$

The equilibrium adsorption capacity is represented by q_e (mg g^{-1}), C_o and C_e are initial and equilibrium Dc concentrations (mg L^{-1}), respectively. V is the volume of the solution (L) and W is the dry weight of the adsorbent (g). While the value of adsorption at time t q_t (mg g^{-1}). In order to get values from the Dc, the measurements were taken in triplicates, and then the mean values were calculated and used for further analysis. The adsorption processes for Dc on adsorbents are shown in scheme 1.

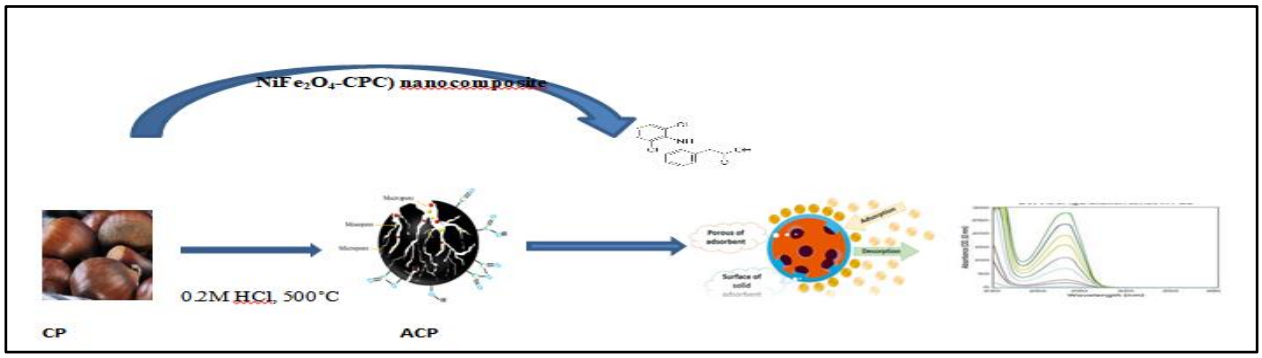

Scheme 1: Adsorption processes for Dc on Adsorbents

3. Results and Discussion

3.1. FT-IR spectrum

The FTIR spectra demonstrated in Figure 2. (a) for the modified Chestnut peels (CP), (ACSPC), and ($NiFe_2O_4$-CPC) nanocomposite (a) before adsorption, (b) after adsorption of Dc respectively, were recorded by FTIR spectrometer between 400 cm^{-1} and 4000 cm^{-1}. FTIR spectra of CP the bands at: 3309.85 cm^{-1},(3566.38-3275.13) cm^{-1}, was attributed to the O-H stretching. The peak of the C=O, N-H bend, -NO_2 aromatic amines vibration is observed at about (1737.86 -1747.51) cm^{-1}, (1604.77-1608.63)cm^{-1}, 1525.64cm^{-1}, 1452.40cm^{-1}. This peak shows that the compounds are of aldehyde, ketone and acid groups, or indicate the C-H was due to carbonyl groups (C=O), N-H bending [24]. The band refers to the –NO stretch of nitrogen-containing compounds and the –CO stretch of carbonyl compounds was observed at around (1317.38-1363.60) cm^{-1}, while the band (1207.44-1269.16) cm^{-1}. The band positioned at 1155.36 cm^{-1}, (1103.28-1157.24)cm^{-1} refers to C-C stretching. The band positioned at 1028.05 cm^{-1}, and 1031.92cm^{-1} refers to the –CN stretch of aliphatic amines. The band (823.60- 896.90) cm^{-1} refers to ring stretching or may originate from the N-H, and ring stretching [26]. The band positioned at 632.65 cm^{-1}, and (534.28-599.86) cm^{-1}, and (418.55-457.13) cm^{-1}, as a result of the C-H bending and stretching of halogenated compounds.

FTIR spectra adsorbent ACPC the band at: (3275.13-3566.38) cm^{-1}, 2970.38cm^{-1}, 2237.43cm^{-1}, due to the O-H stretching, C-H of aliphatic hydrocarbons. The bands observed at (1737.86-1747.51) cm^{-1}, 1608.63cm^{-1}, (1525.69-1541.12)cm^{-1}, 1452.40 cm^{-1} (1317.38-1365.60) cm^{-1}, (1205.51-1269.16)cm^{-1} could be attributed to primary and secondary amide or C=O group, C=C bonds, either isolated or conjugated, which is related to the presence of carbonyl groups or aromatic rings, N–H deforming, C=C bending, and C-N stretching, CH_3 in the $NHCOCH_3$ group, and acetates stretching, or nitrate (NO_2) symmetric stretching, and acetyl groups in hemicelluloses vibration respectively. The observed band at (1103.28-1165.00)cm^{-1}, (1076.28-1028.06)cm^{-1}, it was as a result of the stretching of the C-O stretching, or C-C. The observed band at, (823.60-896.90) cm^{-1}, 744.52 cm^{-1}, (601.79-646.15)cm^{-1}, (534.28-592.15) cm^{-1}, (418.55- 457.13)cm^{-1}, excite in both before adsorption processes was attributed to the vibration C-O stretching, stretching of C-H, O-O, and β-glucosidic linkages between the sugar units in hemicelluloses and cellulose, N-H, and ring stretching, SO_3 group, and halogenated compounds stretching respectively [26].

FTIR spectrum for ($NiFe_2O_4$-CPC) nanocomposite the bands around: (3244.27-3566.38)cm^{-1}, (2970.38-2987.74)cm^{-1}, and (2312.65-2380.16)cm^{-1}, attributed to the O-H stretching, C-H of aliphatic hydrocarbons. 1921.10cm^{-1}, (1714.72-1747.51)cm^{-1} 1608.63cm^{-1}, (1500.62-1595.13)cm^{-1}, 1475.54cm^{-1}, (1317.38-1365.60)cm^{-1}, (1205.51-1217.80)cm^{-1}, (1114.86-1197.79)cm^{-1} , could be due to primary and secondary amide or C=O group, C=C bonds, either isolated or conjugated, which are related to the presence of carbonyl groups or aromatic rings, N–H deforming, C=C bending, and C-N stretching, CH_3 in the $NHCOCH_3$ group, and acetates stretching, or nitrate (NO_2) symmetric

stretching, and acetyl groups in hemicelluloses vibration respectively (1608.63-1693.50)cm^{-1} were due to the C=C stretching either isolated or conjugated, C-N, O–H deformation mode of the water molecule, or carbonyl groups stretching before adsorption. –N=N– stretching, –C–N– stretching, -C-O, C-C stretching, acetyl groups in hemicelluloses, –S=O– stretching, C–H in-plane bending vibration of the benzene ring appeared before and after adsorption. The observed band at (518.85-594.08)cm^{-1}, 416.62cm^{-1} is indicative of the stretching of O-O, C-H, N-H, and ring stretching [26].

Compared to the position of adsorbents band intensity of the presence of aromatic amines between (1737.86 -1747.51)cm^{-1}, C-O bonds of Ester between (1205.51-1269.16)cm^{-1}, the isopropyl group $(CH_3)_2CH$- bonds between (1207.44-1269.16) cm^{-1}, and C-N bonds of the nitrile derivatives at (823.60-896.90) cm^{-1}, which could be ascribed to the reaction between the acid, base and C under high temperature. The peaks observed at 2380.16cm^{-1} and 418.55 cm^{-1} appeared after adsorption. Indicating that the –OH, C-H, C-O, C≡ O, and Ni-O groups on adsorbents participated in the Dc removal process. The existence of several functional groups on the surface of adsorbents has an important role in Dc removal from aqueous solution by electrostatic interactions, complexation reactions, and hydrogen bonding [25, 26].

The XRD diffractogram demonstrated in Figure 3 (a) the modified Chestnut peels (CP), (ACSPC), and (II) oxide ($NiFe_2O_4$-CPC) nanocomposite before adsorption, (b) after the Dc adsorption process respectively. X-ray diffractometer in the 2-theta range between 20-90°at an accelerating voltage of 80 kV, the values before and after the adsorption process for Dc were in the range $(15.3\text{-}45.8)^o$, $(25.7\text{-}41)^o$, $(18.8\text{-}75.5)^o$, $(15.3\text{-}44.1)^o$, $(21.1\text{-}41.95)^o$, and $(18.7\text{-}75.3)^o$ respectively. While the peak observed at 75 ^{o} is assigned to cubic Ni-O crystallites. Applying Scherrer's formula to calculate average diameter values of metal oxide nanoparticles it ranged from (19 -42) nm. It is evident from the diffraction peaks showing the high precision of the pure crystalline structure adsorbent formation [27, 28].

Scanning electron microscopy (SEM) analysis shown in Figure 4 (a) the modified Chestnut peels (CP), (ACSPC), and (II) oxide ($NiFe_2O_4$-CPC) nanocomposite before adsorption (b) after adsorption process for Dc respectively, were the diameter of the porous were in the range (83.5-105.41)nm, (176.12-88.93)nm, and (102.02-75.04)nm, respectively. To examine its surface morphology and porosity, clearly adsorbents had regular flat shapes with a semi-porous surface homogeneity because there is a good grain distribution. After treatment, the adsorbents become rough due to a large deposition of cubic-shaped nanoparticles. The physical and chemical properties of raw materials used and also the carbonization conditions affected the quality and physicochemical characteristics of adsorbents. The most porous surface structures of the adsorbents provide a good possibility for Dc molecules to adsorb into these pores, and a highly heterogeneous structure which provides a large surface area for adsorption [29].

The energy dispersive X-ray spectrometry (EDX) for the adsorbents is shown in Figure 5 (a) before and (b) after adsorption of Dc, respectively. For the observation of surface microporous structure, prior to scanning the adsorbents were coated with a thin layer of gold to make it conductive to obtaining more information about the microstructure of these adsorbents. The EDX result shows that the percentage weight of the elements: C,

O, K for the modified Chestnut peels (CP), (ACSPC), and ($NiFe_2O_4$-CPC) nanocomposite is in the range (23.71 – 87.77%), (11.28 - 42.28)%, and (0-0.39)% respectively. This was supported by the surface adsorbents with an average size of 42 nm, indicating the successful synthesis of the ($NiFe_2O_4$-CPC) nanocomposite [30].

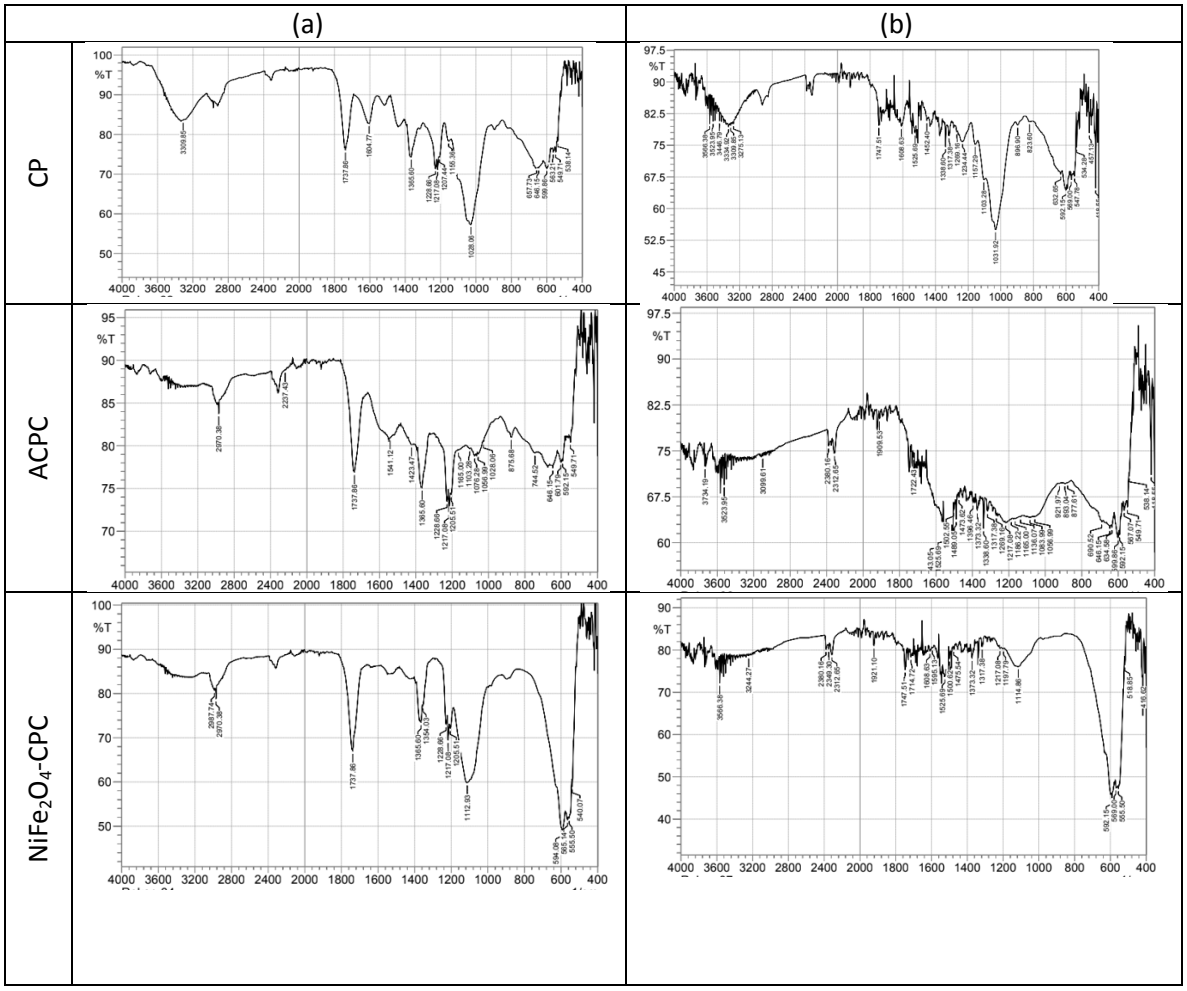

Figure 2. FTIR spectrum of modified chestnut peels (a) before adsorption, (b) after adsorption of Dc respectively.

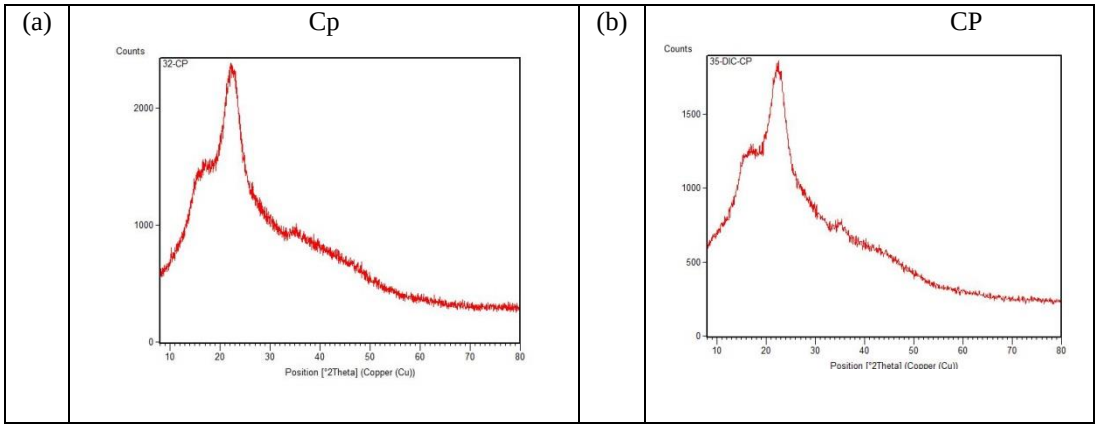

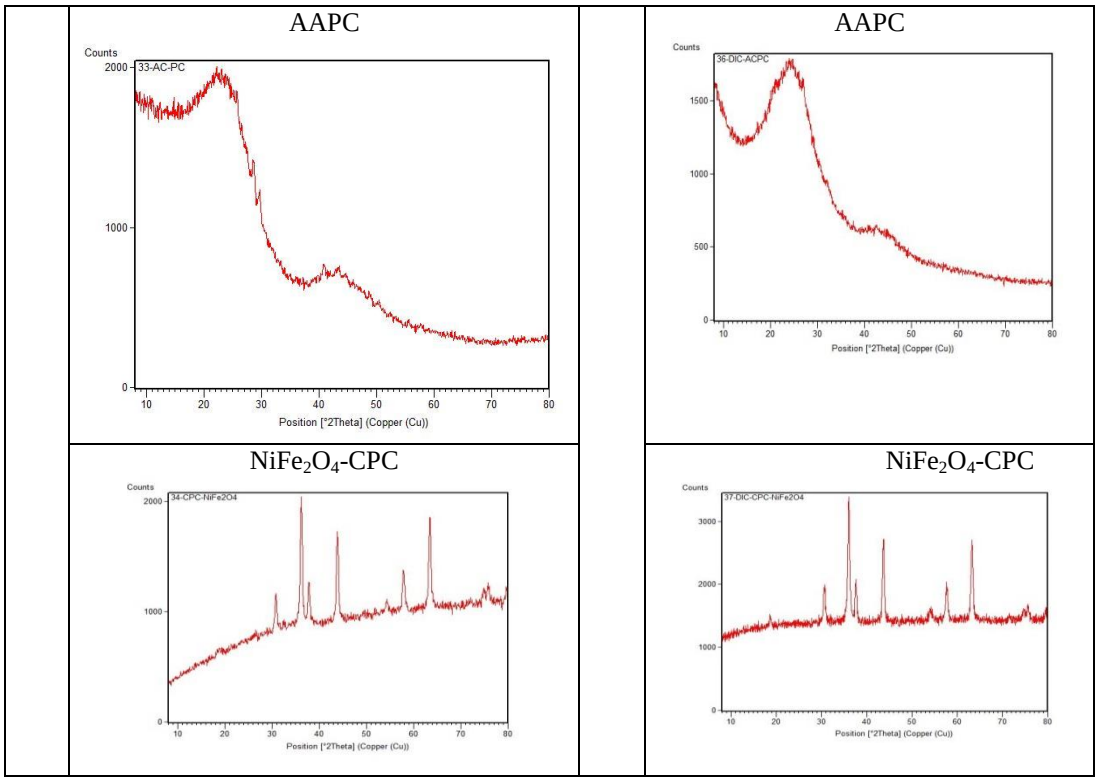

Figure 3. The XRD diffractogram of adsorbents (a) before (b) after adsorption process for Dc respectively.

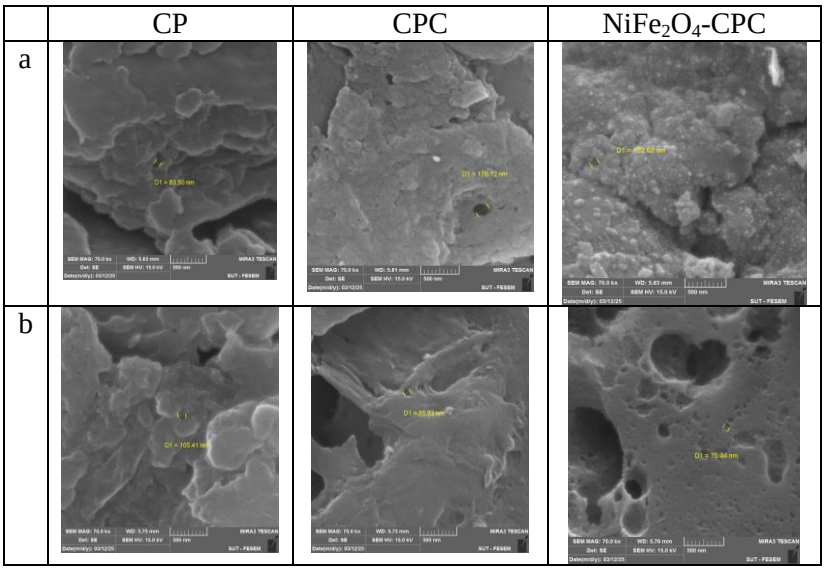

Figure 4 . The SEM micrographs of adsorbents (a) before (b) after adsorption processes for Dc respectively.

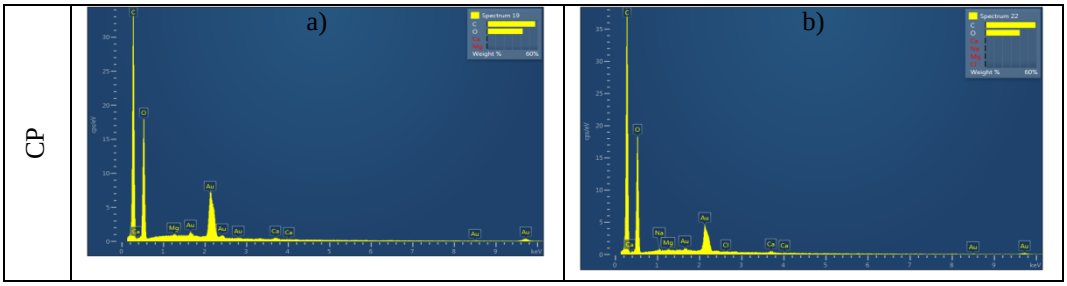

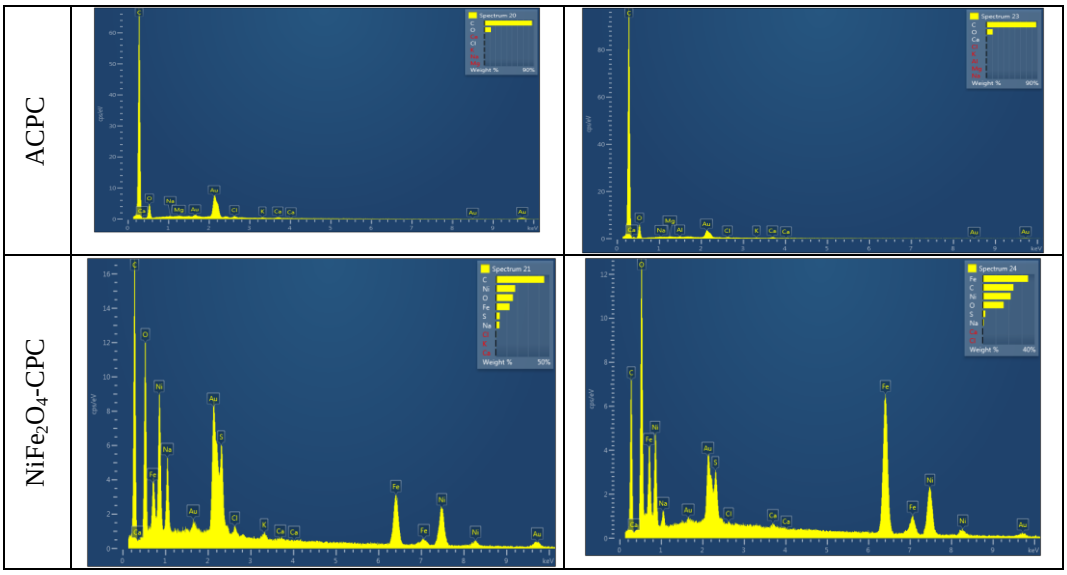

Figure 5 . TheEDX micrographs of adsorbents (a) before (b) after adsorption of Dc respectively.

3.2. Effect of pH

The critical effect on adsorption performance, degree of ionization of the adsorbent's surface functional groups and the adsorbent's surface charge is the pH of the solution. The influence of pH shown in Figure 6 a was investigated for DC solutions at a concentration of 100 mgL^{-1}, which were mixed for 90 min in the solution pH (2-10). An equal amount of adsorbent of 0.05 g of particle size (150 µm) was palsied in a shaker at 170 rpm for the modified Chestnut peels (CP), (ACSPC), and ($NiFe_2O_4$-CPC) nanocomposites, the percentages of adsorbed Dc, were 79.61%, 84.77%, and 92.23% respectively. DC adsorption was less affected by raising the pH of aqueous solution, attributed to increasing negative surface charge of adsorbents and deprotonating of Dc molecules [32].

Zero Charge Point (pH_{PZC}) for the modified Chestnut peels (CP), (ACSPC), and (II) oxide ($NiFe_2O_4$-CPC) nanocomposite were determined by the solid addition method. The value of pH_{pzc} ranged between (6.1- 6.4), as the pH less than pH_{PZC} means that the adsorbent surface will have a positive charge and thus be a surface on which anions may adsorb attributed to the strong gravitational force and the reduction of repulsive force between the adsorbent surface and the Dc. While the adsorbent surface will have a negative charge at pH greater than the pH_{PZC} and thus be a surface on which cations H^+ ions adsorb, the low efficiency of Dc in acidic environments can be[33,34].

3.3. Effect of Dosage

The DC solutions at a concentration of 100 mgL^{-1} were mixed for 90 min with the modified Chestnut peels (CP), (ACSPC), and ($NiFe_2O_4$-CPC) nanocomposite, in amounts (25- 100) mg to determine the effect of dosage on the adsorption processes, and the results are shown in Figure 6 b. The percentages of adsorbed Dc were 82.99%, 86.99%, and 92.04% respectively. Increasing adsorbent dosage caused an increase in percent removal [35].

3.4. Effect of contact time

The contact time variation affecting the quantity of Dc adsorbed per gram of adsorbents was illustrated in Figure c. The adsorption processes for Dc firstly were rapid but then slowed down and attained equilibrium after 90 min attributed to the occupation of active adsorption sites over time. The percentages of adsorbed Dc on modified Chestnut peels (CP), (ACSPC), and ($NiFe_2O_4$-CPC) nanocomposite were 53.38%, 54.99%, 57.29%, 60.74%, and 62.60% respectively. The Dc adsorption was fast at first, but then decreased attributed to the existence of initially empty and easily accessible sites on the surface of the adsorbents, so the adsorption rate became consistent to reach inner pores [36].

3.5. Effect of initial concentration

The effect of the initial Dc concentration of the modified Chestnut peels (CP), (ACSPC), and ($NiFe_2O_4$-CPC) nanocomposite is illustrated in Figure 6 d. As increasing the initial concentrations the adsorbed amount of DC onto adsorbents increased until saturation of adsorbents. The availability of empty adsorption sits on the adsorbent surface due to low initial concentrations of DC. However, it was observed that the adsorption percentages of DC on adsorbents value were 92.73, 95.11, and 98.46 mgL^{-1}, respectively. The adsorption process of Dc was governed by the specific adsorption sites [37].

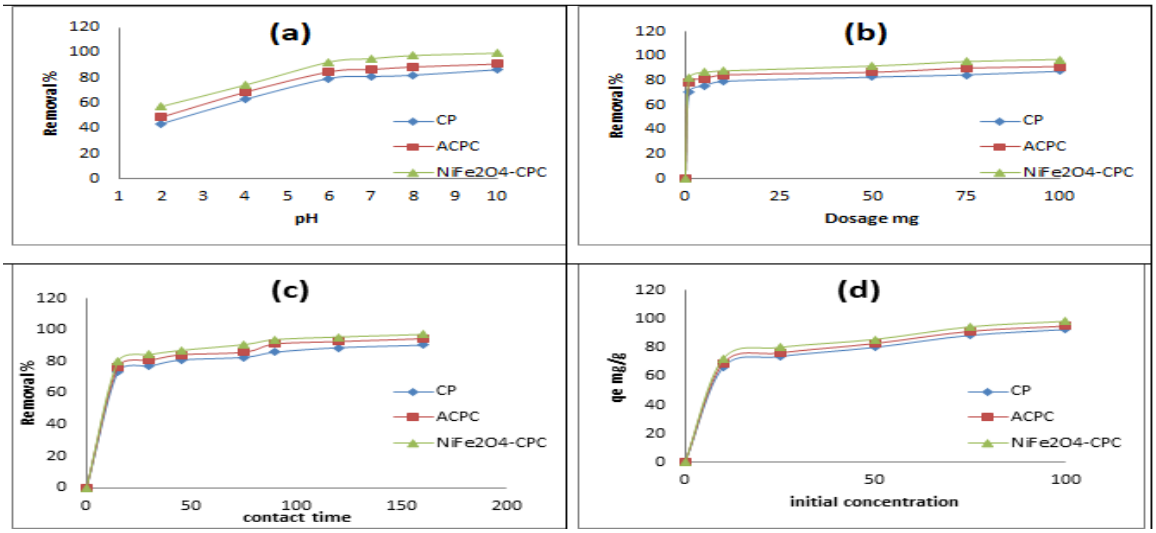

Figure 6. The Effect of (a) pH, (b) dosage, (c) contact time, (d) initial concentration, for the adsorption efficiency of Dc (at an initial concentration of 100 mgL^{-1}, dosage 0.05g, pH 6, contact time of 90 min, and biosorbent size of 150 µm) .by adsorbents at 298K.

3.6. Adsorption Kinetic models

The adsorption kinetic study is the relationship between contact time at equilibrium and the rate. The kinetic study of Dc adsorption onto the modified Chestnut peels (CP), (ACSPC), and ($NiFe_2O_4$-CPC) nanocomposite, was studied using pseudo-first order [38], pseudo-second order [39], and intraparticle diffusion [40], and employing the equations below.

pseudo-first-order; $$\log(q_e - q_t) = \log q_e - \frac{k_1 t}{2.303} \quad (4)$$

pseudo-second-order; $$\frac{t}{q_t} = \frac{1}{k_2 q_e^2} + \frac{t}{q_e} \quad (5)$$

Intraparticle diffusion; $$q_t = K_{id} t^{1/2} + C \quad (6)$$

Where q_t, and q_e denote the amounts of Dc (mg g^{-1}) adsorbed at time t (min) and at equilibrium, respectively. k_1 is the pseudo-first order rate constant (min^{-1}), and determined from plots of $\ln(q_e - q_t)$ versus t for various concentrations of the Dc at different temperatures: 298, 308, and 318 k shown in Table 1, and Figure 7.a . The k_1, q_e, and R^2 values varied between 0.019 - 0.024 min^{-1}, 1.34-13.37 mgg^{-1}, and 0.744 to 0.977 respectively. The experimental differed from the calculated so mention that the removal process does not follow first-order kinetics, the adsorption occurred on the surface functional group [41].

The pseudo-second order rate constant k_2 unit (g mg^{-1} min^{-1}), while q_e can be determined from the slope and intercept of the t/q versus t plot, was illustrated in Tables 1, and Figure 7.b, at different temperatures 298, 308, and 318 k. The k_2, q_e, and R^2 values varied between 0.303 to 1.20 g μg^{-1} min^{-1}, 0.039 to 0.160 mg g^{-1}, and 0.712 to 0.972, respectively. Linearity of the plot, and the alignment of experimental, $R^2 > 0.5$, and calculated q_e values, conditions for applying the second-order kinetics to be the best fits to the analyzed data[42].

The intraparticle diffusion rate constant is K_{id} ($mg \cdot g^{-1} \cdot min^{-1/2}$), while the boundary layer thickness constant is c ($mg \cdot g^{-1}$). The constants K_{id} and c were determined from the slope and intercept of the q_t versus. $t^{1/2}$ graphs. Intraparticle diffusion model graphs for Dc adsorption by adsorbents at 298, 308, and 318 k were demonstrated in Tables 1, and Figure 7.c. The K_{id} , C and R^2 values varied between 0.195 to 0.762 mg g^{-1} $min^{-1/2}$, 7.888 to 58.85 mg g^{-1} and 0.741 to 0.992, respectively. The removal mechanism and the rate control step are investigated by the intraparticle diffusion model, which explains the passage of the Dc from solution to solid surface (film diffusion) and Dc transition to the interior of adsorbent particles (intraparticle diffusion), finally to the interior of adsorbent pores[43].

Table 1: Pseudo first, second order rate constants, and intraparticle diffusion, for adsorption of Dc on adsorbents at 298, 308, and 318K.

temp	Adsorbent	Conc.	Pseudo first order rate			Pseudo second order rate			Intra particle diffusion		
			K min^{-1}	$q_e$mg g^{-1}	R^2	K_2g µg $^{-1}min^{-1}$	$q_e$mg g^{-1}	R^2	K_{id}mg/ g $min^{½}$	C mg g^{-1}	R^2
289K	CP	25	0.020	4.371	0.956	0.568	0.062	0.807	0.342	7.888	0.917
		50	0.021	6.694	0.946	0.515	0.068	0.807	0.460	19.24	0.943
		75	0.021	7.755	0.960	0.429	0.082	0.817	0.566	33.96	0.941
		100	0.021	8.171	0.969	0.399	0.086	0.787	0.574	53.13	0.953
	ACPC	25	0.021	4.010	0.969	0.908	0.039	0.740	0.275	8.209	0.945
		50	0.020	5.352	0.940	0.691	0.048	0.719	0.333	17.72	0.992
		75	0.022	8.141	0.917	0.605	0.054	0.712	0.446	33.21	0.974
		100	0.021	9.001	0.924	0.499	0.066	0.714	0.513	50.20	0.984

	NiFe2O 4-CPC	25	0.021	2.583	0.895	0.977	0.040	0.892	0.289	7.975	0.741
		50	0.021	4.717	0.925	0.664	0.054	0.846	0.372	15.70	0.892
		75	0.021	6.707	0.977	0.541	0.063	0.761	0.466	31.30	0.949
		100	0.021	7.656	0.946	0.464	0.070	0.726	0.489	49.26	0.975
308K	CP	25	0.023	4.873	0.876	0.808	0.047	0.879	0.356	8.956	0.924
		50	0.024	7.055	0.882	0.717	0.051	0.868	0.469	21.62	0.919
		75	0.022	6.917	0.894	0.544	0.068	0.872	0.500	36.43	0.922
		100	0.022	7.463	0.922	0.484	0.075	0.859	0.552	55.43	0.927
	ACPC	25	0.023	3.730	0.918	0.935	0.041	0.897	0.339	9.112	0.863
		50	0.022	5.114	0.875	0.657	0.061	0.891	0.453	19.52	0.887
		75	0.022	5.946	0.903	13.78	0.073	0.888	0.489	35.28	0.913
		100	0.021	6.214	0.886	11.31	0.088	0.892	0.528	54.13	0.915
	NiFe2O 4-CPC	25	0.022	7.725	0.893	0.777	0.041	0.793	0.415	7.960	0.977
		50	0.022	9.213	0.872	0.664	0.049	0.792	0.451	15.94	0.967
		75	0.023	12.46	0.912	0.525	0.062	0.797	0.651	32.42	0.983
		100	0.022	13.37	0.911	0.442	0.073	0.797	0.728	49.50	0.987
318K	CP	25	0.019	1.376	0.744	1.200	0.042	0.972	0.195	11.49	0.793
		50	0.021	2.315	0.751	1.000	0.049	0.970	0.301	23.69	0.797
		75	0.021	2.967	0.768	0.837	0.056	0.964	0.384	39.04	0.798
		100	0.021	4.000	0.866	0.657	0.063	0.928	0.419	58.85	0.838
	ACPC	25	0.024	4.460	0.908	0.935	0.052	0.921	0.322	9.999	0.884
		50	0.024	7.290	0.935	0.510	0.119	0.970	0.446	19.98	0.917
		75	0.024	9.080	0.963	0.333	0.149	0.915	0.562	35.97	0.933
		100	0.024	10.43	0.957	0.303	0.160	0.893	0.631	54.55	0.938
	NiFe2O 4-CPC	25	0.023	4.695	0.854	0.889	0.045	0.877	0.376	9.249	0.905
		50	0.023	6.731	0.886	0.671	0.055	0.865	0.453	17.89	0.912
		75	0.023	8.861	0.971	0.540	0.062	0.751	0.559	34.96	0.958
		100	0.022	9.883	0.958	0.444	0.075	0.743	0.606	54.34	0.966

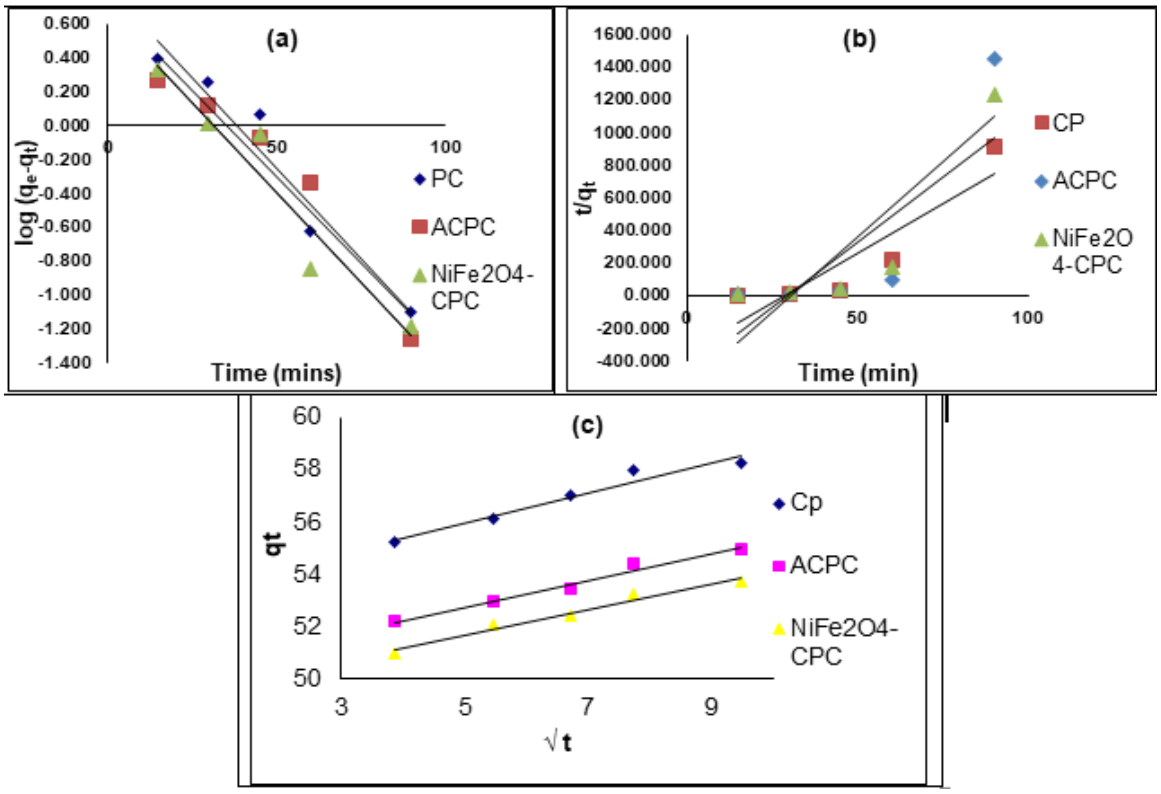

Figure 7.(a) Pseudo-first order (b) Pseudo-second order (c)The intraparticle diffusion models for the adsorption of the Dc using adsorbents at 298K.

3.8. Adsorption Isotherm Study

Adsorption isotherms reveal the relationship between interactions at constant temperature. The interactions between Dc and the modified Chestnut peels (CP),

(ACSPC), and ($NiFe_2O_4$-CPC) nanocomposite were investigated and performed by applying Freundlich [44], Langmuir[45], and Dubinin–Radushkevich [46], and employing the equations below.

Freundlich; $$\ln q_e = \ln k_F + \frac{1}{n}\ln c_e \quad (7)$$

Langmuir; $$\frac{C_e}{q_e} = \frac{1}{K_L q_e} + \frac{C_e}{q_m} \quad (8)$$

$$R_L = \frac{1}{1 + K_L C_o} \quad (9)$$

Dubinin-Radushkevich; $$\ln q_e = \ln q_m - \beta\varepsilon^2 \quad (10)$$

$$\varepsilon = RT \ln(1 + \frac{1}{C_e}\ ) \quad (11)$$

$$E = \frac{1}{\sqrt{2\beta}} \quad (12)$$

Where, q_e (mg g^{-1}) indicates the amount of Dc packed onto the adsorbent at equilibrium, the Freundlich constant represented by K_F [$(mg\cdot g^{-1})(mg\cdot L^{-1})^{1/n}$] and n considers the amplitude and intensity of the removal. The n value is considered as dimensionless adsorption adversity. The Freundlich constants and associated correlation coefficients at 298, 308, and 318 k were demonstrated in Tables 2, and Figure 8.a. The K_F, n_F, and R^2 values varied between 25.96–28.33 mgg^{-1}, 1.322–1.507, 0.889–0.975, respectively.

The Langmuir isotherm defines C_e (mg L^{-1}) as the equilibrium concentration of the Dc, q_e (µg g^{-1}) as the amount of Dc adsorbed per unit mass of adsorbent, and C_{max} and b as the Langmuir constants related to the monolayer adsorption amplitude and the adsorbent's affinity at the Dc, respectively. The graphs of C_e/q_e against C_e, a straight line with a slope of $1/C_{max}$ were acquired, indicating that Dc adsorption on the adsorbents follows the Langmuir isotherm. Where, q_{max} (µg g^{-1}) represents the maximum monolayer adsorption capacity corresponding to site saturation, and K_L (Lmg^{-1}) is the Langmuir isotherm constant, indicating the adsorbent's affinity for the Dc. These values were determined at different temperatures 298, 308, and 318 k and are recorded in Tables 2, as well as Figure 8.b. The K_L, q_{max}, R^2, R_L values varied between 0.014–0.023 L mg^{-1}, 14.286-16.667 mgg^{-1}, 0.737-0.982, and 0.294–0.423 respectively. The Langmuir was monolayer adsorption that occurs on of Dc molecules on the surface of modified Chestnut peels (CP), (ACSPC), and ($NiFe_2O_4$-CPC) nanocomposite, and the highest R^2 values confirm it's the

best fit. The R_L value signalizes and is favorable for Dc adsorption under the conditions applied.

In the Dubinin–Radushkevich model as β is the isotherm constant associated with the adsorption energy ($mol^2 \cdot kJ^2$), q_m is the theoretical adsorption capacity ($mol \cdot g^{-1}$), and ε is the Polanyi potential related to equilibrium concentration. The q_{maxDR} and K_{DR} refer to the Dubinin–Radushkevich maximum monolayer adsorption capacity ($mg\ g^{-1}$) and isotherm constant ($mol^2\ kJ^{-2}$), respectively. R is the gas constant ($8.314\ Jmol^{-1}K^{-1}$) and T represents temperature. The Dubinin–Radushkevich parameters were evaluated at various temperatures (25, 35, and 45±1°C) and are demonstrated in Table 2, and Figure 8.c. The q_{max}, $\mathbf{K_{DR}}$, E, and R^2 values varied between 9.237-9.440, 0.006-0.008, 11.63-17.54, 0.883-4.15, and 0.964-0.999, respectively.

Table2. Adsorption Isotherm parameters for the models Freundlich, Langmuir and Dubinin–Radushkevich for Dc using adsorbents at 298 , 308, and 318 K.

Temp		298 K.			308K			318 K		
Ads mod	Parameter	CP	ACPC	$NiFe_2O_4$-CPC	CP	ACPC	$NiFe_2O_4$-CPC	CP	ACPC	$NiFe_2O_4$-CPC
Freundlich	K_F mg/g)(L/mg)$^{1/n}$	27.80	27.91	28.33	26.46	26.64	27.16	25.62	25.96	26.56
	n_F	1.507	1.458	1.474	1.388	1.371	1.385	1.327	1.322	1.359
	R^2	0.975	0.947	0.906	0.984	0.952	0.877	0.964	0.936	0.889
Langmuir	K_L (L/mg)	0.023	0.021	0.024	0.015	0.017	0.019	0.014	0.015	0.017
	q_m(mg/g)	14.286	14.286	16.667	16.667	16.667	16.667	16.667	16.667	16.667
	R_L	0.300	0.318	0.294	0.394	0.369	0.348	0.423	0.400	0.375
	R^2	0.982	0.926	0.872	0.971	0.893	0.737	0.894	0.810	0.737
Dubinin–Radushkevich	q_{max} (mg/g)	9.266	9.376	9.440	9.237	9.328	9.425	9.243	9.345	9.377
	K_{DR} (mol^2/j^2)	0.006	0.006	0.006	0.007	0.007	0.007	0.008	0.008	0.007
	E(Kj/mol)	11.63	12.12	14.09	10.99	15.39	15.15	11.63	17.54	17.24
	R^2	0.996	0.996	0.986	0.989	0.999	0.964	0.999	0.995	0.974

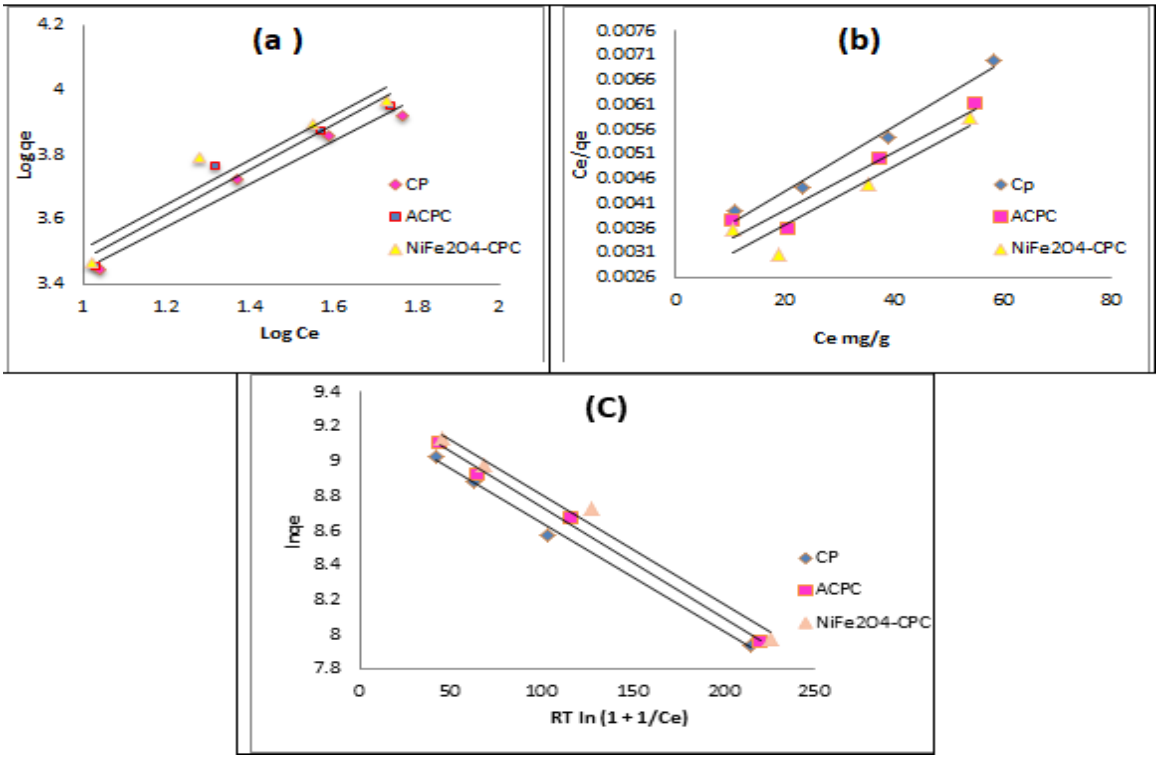

Figure 8 Adsorption isotherm models (a) Freundlich, (b) Langmuir (c) Dubinin–Radushkevich, for the adsorption of the Dc using adsorbents at 298K

3.7 Adsorption Thermodynamic Study

The adsorption thermodynamic of Dc by the modified Chestnut peels (CP), (ACSPC), and ($NiFe_2O_4$-CPC) nanocomposites was conducted. The investigation of the effect of temperature on the adsorption reveals more significant information about the thermodynamic parameters: Gibbs free energy change (ΔG^o), enthalpy change (ΔH^o), and entropy change (ΔS^o) [47]. The thermodynamic equations are as follows.

$$\Delta G^o = -RT \ln K_o \qquad (13)$$

$$LnK_o = \frac{\Delta S^o}{R} - \frac{\Delta H^o}{RT} \qquad (14)$$

Where T, R, and K^o are absolute temperature (K), universal gas constant (8.314 $JK^{-1}mol^{-1}$), and thermodynamic constant [are obtained from binding Langmuir constant (K_Lx C^o), where C^o is the reference concentration], respectively. The value of ΔH^o and ΔS^o of the adsorption processes can be calculated from the slope and the intercept of the graph of ln K_o versus T^{-1}, and demonstrated in Table 3 and Figure 9. The K_o, E_a, ΔG^o, ΔH^o, ΔS^o and R^2 values varied between 14000–24000, 10.74-17.24 $KJmol^{-1}$, -25.77 to -24.70 $KJmol^{-1}$, -19.72 to - 13.30 $KJmol^{-1}$, 0.169 to 0.381 $KJmol^{-1}K^{-1}$, 0.865 - 0.967, respectively. The negative value is less than 40 $kJ{\cdot}mol^{-1}$ for ΔH^o which suggests an exothermic and a phyisorption process. The positive of ΔS^o value specified an increase in the probability of randomness at the solid–liquid interface during the adsorption of Dc ion onto all the modified Chestnut peels (CP), (ACSPC), and ($NiFe_2O_4$-CPC) nanocomposites. When

temperature increased ΔG^o was going to get a negative value and the processes were spontaneous [48].

Table3. The Free energy change, standard entropy change and standard enthalpy change for adsorption of Dc on adsorbents at three temperatures.

Tem K	Parameter	CP	ACPC	$NiFe_2O_4$-CPC
298	K^o	23000	21000	24000
	ΔG (kJ/mol	-24.90	-24.70	-25.00
308	K^o	15000	17000	19000
	ΔG (kJ/mol	-24.64	-24.95	-25.24
318	K^o	14000	15000	17000
	ΔG (kJ/mol	-25.25	-25.43	-25.77
ΔH (kJ/mol)		-19.72	-13.30	-13.65
ΔS (J/mol. K)		0.169	0.381	0.380
Ea (kJ/mol)		17.24	10.74	10.99
R^2		0.865	0.984	0.967

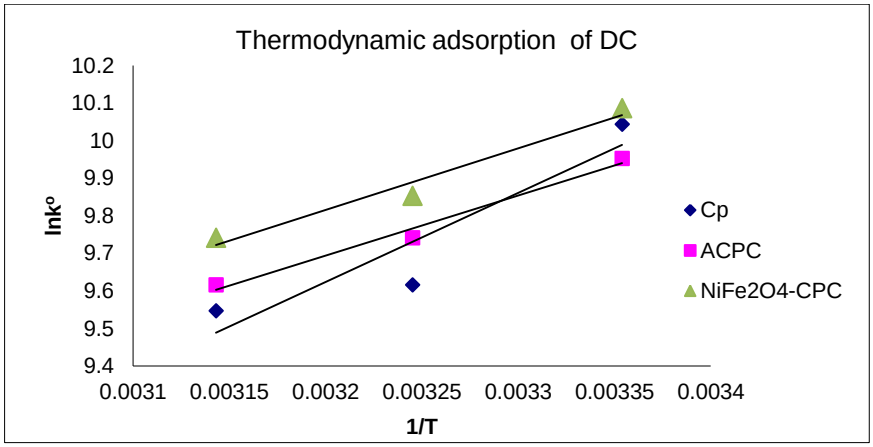

Figure 9. The alteration of ln K^o with 1/T for adsorption of Dc on adsorbents.

4. Conclusions

The modified Chestnut peels (CP), (ACSPC), and ($NiFe_2O_4$-CPC) nanocomposites were investigated to remove Dc from an aqueous solution. The consequence showed that adsorbents have a crystalline structure and size of 20-25 nm. The description results of FTIR, XRD, SEM, and EDX, analysis demonstrating successful adsorption of Dc on the adsorbents. Langmuir and Pseudo's second order equation was well fitted with isotherm data, and with the maximum adsorption capacity. The thermodynamic parameters confirmed the spontaneous and endothermic process. The regeneration of adsorbents was efficient and showed high removal of Dc from aqueous solution in five consecutive cycles using buffer solution pH 6. This characteristic is particularly advantageous in industries where elevated temperatures are common, such as in wastewater treatment and chemical manufacturing; this enhances the efficiency of adsorption. Advantage of the prepared

adsorbents from agricultural waste approved industrially and in wastewater treatment, which enhances the adsorption efficiency and is eco-friendly.

.

Acknowledgements

I would like to thank the Salahaddin University-Erbil, Kurdistan Region, Iraq for financially supporting this study.

References

[1] Tran, N. H., Reinhard, M., Khan, E., Chen, H., Nguyen, V. T., Li, Y., Goh, S. G., Nguyen, Q. B., SaeidI, N. & GiN, K. Y.-H. [2019]: Emerging contaminants in wastewater, stormwater runoff, and surface water: Application as chemical markers for diffuse sources. Science of the Total Environment, 676, pp. 252-267.

[2] Gomes, A. R., Justino, C., Rocha-santos, T., Freitas, A. C., Duarte, A. C. & Pereira, R. [2017]: Review of the ecotoxicological effects of emerging contaminants to soil biota. Journal of environmental science and health, Part A, 52, pp. 992-1007.

[3] Álvarez, S., Ribeiro, R. S., Gomes, H. T., SotelO, J. L. & García, J. [2015]: Synthesis of carbon xerogels and their application in adsorption studies of caffeine and diclofenac as emerging contaminants. Chemical Engineering Research and Design, 95, pp. 229-238.

[4] Onaga Medina, F. M., Aguiar, M. B., Parolo, M. E. & Avena, M. J. [2021]: Insights of competitive adsorption on activated carbon of binary caffeine and diclofenac solutions. J Environ Manage, 278, pp. 111523.

[5] Barrios, J. A., Cano, A., Becerril, J. E. & Jimenez, B. [2016]. Influence of solids on the removal of emerging pollutants in electrooxidation of municipal sludge with boron-doped diamond electrodes. Journal of Electroanalytical Chemistry, 776, pp. 148-151.

[6] Cero, J. L., Benitez, F. J., Real, F. J. & Rodriguez, E. [2015]: Elimination of selected emerging contaminants by the combination of membrane filtration and chemical oxidation processes. Water, Air, & Soil Pollution, 226, pp. 1-14.

[7] Rafatullah, M., Sulaiman, O., Hashim, R. & Ahmad, A. [2009]: Adsorption of copper (II), chromium (III), nickel (II) and lead (II) ions from aqueous solutions by meranti sawdust. Journal of hazardous materials, 170, pp. 969-977.

[8] Kumar, P. S., Joshiba, G. J., Femina, C. C., Varshini, P., Priyadharshini, S., Karthick, M. A. & Jothirani, R. [2019]: A critical review on recent developments in the low-cost adsorption of dyes from wastewater. Desalination and Water Treatment, 172, pp. 395-416.

[9] Prasannamedha, G., Kumar, P. S., Mehala, R., Sharumitha, T. & SURENDHAR, D. [2021]: Enhanced adsorptive removal of sulfamethoxazole from water using biochar derived from hydrothermal carbonization of sugarcane bagasse. Journal of Hazardous Materials, 407, pp. 124825.

[10] Naghipour, D., Hoseinzadeh, L., Taghavi, K. & Jaafari, J. [2018]: Characterization, kinetic, thermodynamic and isotherm data for diclofenac removal from aqueous solution by activated carbon derived from pine tree. Data in brief, 18, pp. 1082-1087.

[11] Malhotra, M., Suresh, S. & Garg, A. [2018]: Tea waste derived activated carbon for the adsorption of sodium diclofenac from wastewater: adsorbent characteristics, adsorption isotherms, kinetics, and thermodynamics. Environmental Science and Pollution Research, 25, pp. 32210-32220.

[12] Bernardo, M., Rodrigues, S., Lapa, N., MatoS, I., Lemos, F., BatistA, M., CarvalhO, A. & Fonseca, I. [2016]: High efficacy on diclofenac removal by activated carbon produced from potato peel waste. International journal of environmental science and technology, 13, pp. 1989-2000.

[13] Vedenyapina, M., Stopp, P., Weichgrebe, D. & Vedenyapin, A. [2016]: Adsorption of diclofenac sodium from aqueous solutions on activated carbon. Solid Fuel Chemistry, 50, pp. 46-50.

[14] Fernandez, M. E., Ledesma, B., Román, S., Bonelli, P. R. & Cukierman, A. L. [2015]: Development and characterization of activated hydrochars from orange peels as potential adsorbents for emerging organic contaminants. Bioresource technology, 183, pp. 221-228.

[15] Wong, S., Lim, Y., Ngadi, N., Mat, R., Hassan, O., Inuwa, I. M., MohameD, N. B. & Low, J. H. [2018]: Removal of acetaminophen by activated carbon synthesized from spent tea leaves: equilibrium, kinetics and thermodynamics studies. Powder Technology, 338, pp. 878-886.

[16] Esmaeeli, F., Gorbanian, S. A. & Moazezi, N. [2017]: Removal of estradiol valerate and progesterone using powdered and granular activated carbon from aqueous solutions. International Journal of Environmental Research, 11, pp. 695-705.

[17] Li, D., Chen, L., Zhang, X., YE, N. & Xing, F. [2011]: Pyrolytic characteristics and kinetic studies of three kinds of red algae. Biomass and Bioenergy, 35, pp. 1765-1772.

[18] Leite, A. B., Saucier, C., Lima, E. C., Dos Reis, G. S., Umpierres, C. S., MellO, B. L., Shirmardi, M., DiaS, S. L. & Sampaio, C. H. [2018]: Activated carbons from avocado seed: optimisation and application for removal of several emerging organic compounds. Environmental Science and Pollution Research, 25, pp. 7647-7661.

[19] Khoshhesab, Z. M., Ayazi, Z. & Farrokhrouz, Z. [2016]: Ultrasound-assisted mixed hemimicelle magnetic solid phase extraction followed by high performance liquid chromatography for the quantification of atorvastatin in biological and aquatic samples. Analytical Methods, 8(24), pp.4934-4940.

[20] Ayazi, Z., Khoshhesab, Z. M. & Norouzi, S. [2016]: Modeling and optimizing of adsorption removal of Reactive Blue 19 on the magnetite/graphene oxide nanocomposite via response surface methodology. Desalination and Water Treatment, 57(52), 25301-25316.

[21] Deraz, N., Alarifi, A. & Shaban, S. [2010]: Removal of sulfur from commercial kerosene using nanocrystalline NiFe2O4 based sorbents. Journal of Saudi Chemical Society, 14(4), pp. 357-362.

[22] Zandipak R, Sobhanardakani S. Synthesis of $NiFe_2O_4$ nanoparticles for removal of anionic dyes from aqueous solution. Desalination and Water Treatment. 2016; 57 (24):11348-60.

[23] Gunjakar, J., More, A., Gurav, K. & Lokhande, C. [2008]: Chemical synthesis of spinel nickel ferrite (NiFe2O4) nano-sheets. Applied Surface Science, 254(18), pp. 5844-5848.

[24] Bouhcain, B., Carrillo-Peña, D., El MansourI, F., Ez zoubi, Y., Mateos, R., Morán, A., Quiroga, J. M. & Zerrouk, M. H. [2022]: Removal of emerging contaminants as diclofenac and caffeine using activated carbon obtained from argan fruit shells. Applied Sciences, 12, pp. 2922

[25] Ayazi, Z., MonseF Khoshhesab, Z. & Amani-Ghadim, A. [2018]: Synthesis of nickel ferrite nanoparticles as an efficient magnetic sorbent for removal of an azo-dye: Response surface methodology and neural network modeling. Nanochemistry Research, 3(1), pp.109-123.

[26] Thommes, M., Kaneko, K., Neimark, A. V., Olivier, J. P., Rodriguez-Reinoso, F., RouqueroL, J. & Sing, K. S. [2015]: Physisorption of gases, with special reference to the evaluation of surface area and pore size distribution (IUPAC Technical Report). Pure and applied chemistry, 87, pp. 1051-1069.

[27] Gan, T., Zhang, Y., SU, Y., Hu, H., Huang, A., Huang, Z., Chen, D., Yang, M. & Wu, J. [2017]: Esterification of bagasse cellulose with metal salts as efficient catalyst in mechanical activation-assisted solid phase reaction system. *Cellulose*, 24(12)**,** pp. 5371-5387.

[28] Sharma, A. K., Desnavi, S., Dixit, C., Varshney, U. & Sharma, A. [2015]: Extraction of nickel nanoparticles from electroplating waste and their application in production of bio-diesel from biowaste. *International Journal of Chemical Engineering and Applications*, 6(3), pp. 156-160.

[29] Qamar, M., Gondal, M. & Yamani, Z. [2011]: Synthesis of nanostructured NiO and its application in laser-induced photocatalytic reduction of Cr (VI) from water. Journal of Molecular Catalysis A: Chemical, 341, pp. 83-88.

[30] Albokheet, W., Gouda, M. & AL-Faiyz, Y. [2021]: Removal of Methylene Blue Dye Using Nickel Oxide/Carboxymethyl Cellulose Nano composite: Kinetic, Equilibrium and Thermodynamic Studies. Journal of Textile Science & Fashion Technology, 8(2), pp. 1-10.

[31] Umair Baig, Mohammad Kashif Uddin, M.A. Gondal, Removal of Hazardous Azo Dye from Water Using Synthetic Nano Adsorbent: [2016]: Facile Synthesis, Characterization, Adsorption, Regeneration and Design of Experiments. Colloids and Surfaces A: Physicochemical and Engineering Aspects, 23, pp. 116-1232.

[32] Hadra, B. N., Seo, P. W. & Jhung, S. H. [2016]: Adsorption of diclofenac sodium from water using oxidized activated carbon. Chemical Engineering Journal, 301, pp. 27-34.
[33] Omer, O. S., Hussein, M. A., Hussein, B. H. & Mgaidi, A. [2018]: Adsorption thermodynamics of cationic dyes (methylene blue and crystal violet) to a natural clay mineral from aqueous solution between 293.15 and 323.15 K. Arabian Journal of Chemistry, 11, pp. 615-623.
[34] Foroutan, R., Peighambardoust, S. J., Peighambardoust, S. H., Pateiro, M. & Lorenzo, J. M. [2021]: Adsorption of crystal violet dye using activated carbon of lemon wood and activated carbon/Fe3O4 magnetic nanocomposite from aqueous solutions: a kinetic, equilibrium and thermodynamic study. Molecules, 26, pp. 2241.
[35] Gundoğdu, A., Şenturk, H. B., Duran, C., İmamoğlu, M. & SOYLAK, M. [2018]: A new low-cost activated carbon produced from tea-industry waste for removal of Cu (II) ions from aqueous solution: Equilibrium, kinetic and thermodynamic evaluation. Karadeniz Chemical Science and Technology, 2, pp. 1–10.
[36] Ozer, C. & Imamoglu, M. [2017]: Adsorptive transfer of methylene blue from aqueous solutions to hazelnut husk carbon activated with potassium carbonate. Desalination and Water Treatment, 94, pp. 236-243.
[37] Usanmaz, S., Özer, Ç. & İmamoğlu, M. [2021]: Removal of Cu (II), Ni (II) and Co (II) ions from aqueous solutions by hazelnut husks carbon activated with phosphoric acid. Desalination and Water Treatment, 227, pp. 300-308.
[38] Lagergren S., About [1898]: the theory of so-called adsorption of soluble substances, Kongl. Vetensk. Acad. Handl., 24, pp. 1–39.
[39] HO, Y.-S. & MCKAY, G. [1999]: Pseudo-second order model for sorption processes. Process biochemistry, 34, pp.451-465.
[40] Weber JR, W. J. & Morris, J. C. [1963]: Kinetics of adsorption on carbon from solution. Journal of the sanitary engineering division, 89, pp. 31-59.
[41] Rizzo, L., Malato, S., Antakyali, D., Beretsou, V. G., Đolić, M. B., Gernjak, W., Heath, E., Ivancev-Tumbas, I., Karaolia, P. & Ribeiro, A. R. L. [2019]: Consolidated vs new advanced treatment methods for the removal of contaminants of emerging concern from urban wastewater. Science of the Total Environment, 655, pp. 986-1008.
[42] Antunes, M., Esteves, V. I., Guegan, R., Crespo, J. S., Fernandes, A. N. & Giovanela, M. [2012]: Removal of diclofenac sodium from aqueous solution by Isabel grape bagasse. Chemical Engineering Journal, 192, pp.114-121.
[43] Karacetin, G., Sivrikaya, S. & Imamoğlu, M. [2014]: Adsorption of methylene blue from aqueous solutions by activated carbon prepared from hazelnut husk using zinc chloride. Journal of Analytical and Applied Pyrolysis, 110**,** pp. 270-276.
[44] Fan, S., Tang, J., Wang, Y., LI, H., Zhang, H., Tang, J., Wang, Z. & LI, X. [2016]: Biochar prepared from co-pyrolysis of municipal sewage sludge and tea waste for the adsorption of methylene blue from aqueous solutions: Kinetics, isotherm, thermodynamic and mechanism. Journal of Molecular Liquids, 220, pp.432-441.
[45] Shirani, Z., Santhosh, C., Iqbal, J. & Bhatnagar, A. [2018]: Waste Moringa oleifera seed pods as green sorbent for efficient removal of toxic aquatic pollutants. Journal of environmental management, 227, pp.95-106.
[46] Dubinin, M. & Radushkevich, L. Evaluation of microporous materials with a new isotherm. Dokl. Akad. Nauk. SSSR, [1947], pp. 331-334.
[47] De luna, M. D. G., Budianta, W., Rivera, K. K. P. & Arazo, R. O. [2017]: Removal of sodium diclofenac from aqueous solution by adsorbents derived from cocoa pod husks. Journal of Environmental Chemical Engineering, 5, pp.1465-1474.
[48] Tunay, S., Köklu, R. & İmamoğlu, M. [2022]: Removal of diclofenac, ciprofloxacin and sulfamethoxazole from wastewater using granular activated carbon from hazelnut shell: isotherm, kinetic and thermodynamic studies. Desalination and Water Treatment, 277, pp. 155-168.